Separation and Purification Technology 349 (2024) 127831

Contents lists available at ScienceDirect

Separation and Purification Technology

journal homepage: www.elsevier.com/locate/seppur

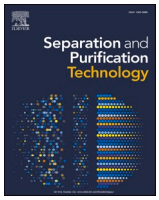

Quantitative image analysis for assessing extracellular polymeric substances in activated sludge under atrazine exposure

Antonio Melo [a], Joana Costa [a], Cristina Quintelas [a,b], António L. Amaral [a,c,d], Eugénio C. Ferreira [a,b], Daniela P. Mesquita [a,b,*]

[a] CEB – Centre of Biological Engineering, University of Minho, 4710-057 Braga, Portugal
[b] LABBELS – Associate Laboratory, Braga/Guimarães, Portugal
[c] Polytechnic Institute of Coimbra, Coimbra Institute of Engineering, Rua Pedro Nunes, Quinta da Nora, 3030-199 Coimbra, Portugal
[d] Research Centre for Natural Resources Environment and Society (CERNAS), Polytechnic Institute of Coimbra, Bencanta, 3045-601 Coimbra, Portugal

ARTICLE INFO

Editor: B. Van der Bruggen

Keywords:
Atrazine
Sequencing batch reactor
Aggregates
Image analysis
Partial least squares

ABSTRACT

Extracellular polymeric substances (EPS) play a vital role in biological wastewater treatment systems. This study investigates the impact of herbicide atrazine (ATZ) on the overall performance, EPS yield, composition, and sludge morphology in an activated sludge (AS) system operated in a sequencing batch reactor (SBR). Since conventional methods for analyzing EPS are time-consuming and releases residues, a new approach was developed in this work to evaluate the EPS fractions and components, based on the morphological characterization of the biomass using quantitative image analysis (QIA) technique coupled with multivariate statistics.

Results showed that exposure to ATZ inhibit biomass activity in terms of organic matter (COD) and nitrogen removal. Moreover, both tightly bound EPS (TB-EPS) and loosely bound EPS (LB-EPS) increased under ATZ, indicating that microorganisms release EPS as a defense mechanism against environmental changes. The PN/PS ratio also increases, indicating likely increased hydrophobicity in ATZ phases. Furthermore, ATZ phases exhibit a predominance of large aggregates compared to intermediate and small ones, indicating a change in aggregate morphological structure associated with EPS production. The new approach using QIA coupled with partial least squares (PLS) modeling provides accurate predictions of EPS content. The increase in TB-EPS is closely related to the rise of large aggregates in phases exposed to higher ATZ concentrations. The PLS models demonstrate high accuracy for EPS prediction (coefficients of determination, R^2 above 0.86), showcasing the feasibility of using QIA for EPS assessment in AS systems. This approach offers significant potential for regular process monitoring and management, providing a more environmentally friendly methodology by eliminating the need for chemical usage.

1. Introduction

Emerging compounds are being released into the environment at an accelerated rate due to the development and complexity of new products manufacturing. Pesticides are widely employed to protect plants from diseases, grass weeds and insect damage [1]. Among pesticides, atrazine (ATZ) is commonly used in agricultural activities [2]. Since 2004, ATZ has been banned for use in the European Union due to concerns over its environmental and health impacts but is still found in groundwater [3]. However, despite this ban, ATZ continues to be used in the United States, as it was recently reapproved for use in the fall of 2020 [4]. As a consequence, ATZ can be found in wastewater treatment plants (WWTP) and natural aquatic environments [5]. Improper discharges from factories, containing highly variable concentrations from 0.1 to 107 mg L^{-1} of these substances, are a significant source of emerging compounds in WWTP and water bodies [6]. Research on the impacts of ATZ in biological wastewater treatment (WWT) is therefore essential, especially in activated sludge (AS), the main biological process employed worldwide.

Extracellular polymeric substances (EPS) are defined as biopolymers of microbial origin which in microbial aggregate systems are frequently responsible for binding cells and other particulate materials [7]. Loosely bound (LB-EPS) and tightly bound (TB-EPS) are EPS fractions, composed mainly by their components, proteins (PN) and polysaccharides (PS). Different roles can be attributed to EPS components influencing the

* Corresponding author at: CEB – Centre of Biological Engineering, University of Minho, 4710-057 Braga, Portugal.
E-mail address: daniela@ceb.uminho.pt (D.P. Mesquita).

https://doi.org/10.1016/j.seppur.2024.127831
Received 21 November 2023; Received in revised form 18 March 2024; Accepted 5 May 2024
Available online 5 May 2024

chemical properties of the aggregates surface, where the PN/PS ratio has been reported as an indicator of hydrophobicity and PN is the leading contributor to this characteristic [8,9]. The features of EPS make them well-suited to take part in the biosorption process by interacting with hazardous molecules, like ATZ, through their functional groups, and allowing bacterial cells to degrade these substances [10]. Additionally, it was previously found that EPS fractions have distinct responses to changes in the microorganisms' environment. Many studies have stated that increasing EPS concentration, mainly in the form of LB-EPS, appears to have a negative effect on bioflocculation properties causing a deterioration in cell adhesion and weakened the aggregate structure, decreasing the capacity of biomass-water separation [11,12].

To assess EPS fractions and components, various extraction methods are commonly employed, along with conventional analytical techniques. These methods are preferred due to their wide availability and established nature compared to more advanced approaches like microscopy or spectroscopy [13]. Nonetheless, the chemical quantification of EPS is a time-consuming process that generates chemical waste. Hence, it is imperative to innovate and develop environmentally friendly monitoring tools.

Quantitative image analysis (QIA) has proven to be a successful tool in studying AS characteristics. Given the multitude of variables inherent in AS monitoring, including operational and QIA parameters, the importance of multivariate statistics, such as partial least squares (PLS), has increased significantly. PLS is specifically designed to manage large datasets, making it particularly valuable for investigating complex biological processes. In this context, PLS coupled to QIA, has been applied in AS systems to estimate effluent chemical oxygen demand (COD), ammonia ($N\text{-}NH_4^+$), and nitrate ($N\text{-}NO_3^-$) concentrations [14]. More recently, in aerobic granular sludge a QIA-based methodology coupled to PLS was used, and it was found good assessment abilities for the effluent COD, $N\text{-}NH_4^+$, $N\text{-}NO_2^-$, $N\text{-}NO_3^-$, salinity (Cl^-), and total suspended solids (TSS) [15].

To overcome the limitations of standard analytical techniques, the current study explores a cutting-edge monitoring approach centered on QIA. This method incorporates chemometrics to integrate image-based parameters assessing biomass structure with traditionally determined EPS fractions and components, aiming to gain a deeper understanding of the complex interactions within the biomass.

2. Material and methods

2.1. Reactor setup and operation

A lab-scale SBR with a 2 L working volume was operated at room temperature (19.5 ± 2.5 °C) in cycles of 6 h as follows: 40 min feeding, 240 min aeration, 40 min sludge settling, and 40 min effluent discharge. Oxygen was supplied (air flow of 2 L min^{-1}) at the bottom during aeration phase to ensure good mixing and saturation with dissolved oxygen. The SBR was inoculated with AS from a municipal WWTP at an initial concentration of 3000 mg/L of mixed liquor suspended solids (MLSS). The sludge retention time was set at approximately 10 days, and the hydraulic retention time was 12 h with a volumetric exchange ratio of 50 %. The reactor was operated at a pH of 7.0 ± 0.6, on average. In the feeding phase, the reactor received a one-litre addition of a synthetic medium containing $NaCH_3COO{\cdot}3H_2O$ (1.450 g L^{-1}), NH_4Cl (0.120 g L^{-1}), K_2HPO_4 (0.028 g L^{-1}), $MgSO_4{\cdot}7H_2O$ (0.030 g L^{-1}), $CaCl_2{\cdot}2H_2O$ (0.07 g L^{-1}), KCl (0.015 g L^{-1}) and a concentrated trace solution (3.5 mL L^{-1}) consisting of: $FeCl_3{\cdot}6H_2O$ (1.5 g L^{-1}); H_3BO_3 (0.15 g L^{-1}); $CuSO_4{\cdot}5H_2O$ (0.03 g L^{-1}); KI (0.18 g L^{-1}); $MnCl_2{\cdot}4H_2O$ (0.12 g L^{-1}); $Na_2MoO_2{\cdot}2H_2O$ (0.06 g L^{-1}); $ZnSO_4{\cdot}7H_2O$ (0.12 g L^{-1}); $CoCl_2{\cdot}6H_2O$ (0.25 g L^{-1}). The SBR was operated for 139 days: phase I (32 days, day 0 to 32) in the absence of ATZ, phase II (32 days, day 35–67), phase III (33 days, day 70–103), and phase IV (33 days, day 106–139) containing ATZ concentrations of 2.1 ± 0.06, 6.1 ± 1.2 and 12.5 ± 2.6 mg L^{-1} each.

2.2. Analytical methods

Chemical oxygen demand (COD), ammonium ($N\text{-}NH_4^+$), nitrite ($N\text{-}NO_2^-$), and nitrate ($N\text{-}NO_3^-$) were determined with Hach Lange cell tests (Hach-Lange GmbH, Dusseldorf, Germany). A Hach Lange HT 200 S thermostat and a Hach Lange DR 2800 spectrophotometer were used in this analysis. The total inorganic nitrogen (TIN) concentration in the influent was assumed to be equal to the ammonium concentration, while the TIN in the effluent was determined as the sum of ammonium, nitrite, and nitrate concentrations. MLSS, mixed liquor volatile suspended solids (MLVSS) and the sludge volume index at 30 min (SVI) were determined in accordance to standard methods [16].

The analysis of ATZ was performed using a Shimadzu apparatus (Shimadzu Corporation, Tokyo, Japan) comprising a Nexera UHPLC system with a Kinetex 5 μ EVO C18 column (150 × 4.6 mm i.d.) provided by Phenomenex, Inc. (CA, USA). The system includes a multi-channel pump (LC-30 CE), an autosampler (SIL-30AC), an oven (CTO-20AC), a diode array detector (M-20A), and a system controller (CBM-20A) with built-in software (LabSolutions). The mobile phase consisted of water (pump A) and acetonitrile (pump B). An isocratic method was employed using 15 % A and 85 % B. The flow rate was set to 1.0 mL min^{-1}. The samples were monitored in the range of 190–400 nm, and chromatograms were extracted at 220 nm. The column oven was maintained at 25 °C, and the injection volume was 30 μL [17].

2.3. EPS extraction and quantification

LB-EPS and TB-EPS were extracted from sludge using a heat extraction method. Initially, a sludge suspension was dewatered through centrifugation (5810 R, Eppendorf) in a 40 mL tube at 8000 g for 5 min. The resulting sludge pellet was then resuspended in a 100 mM NaCl solution, maintaining the original volume of 40 mL, with the NaCl solution having a salinity similar to that of the SBR reactor solution. To ensure rapid heating of the sludge suspension, the NaCl solution for dilution was preheated to 70 °C, thereby achieving a temperature of 50 °C for the sludge suspension. The sludge suspension was sheared using a vortex mixer for 1 min and subsequently centrifuged at 4000*g* for 10 min. The organic matter present in the supernatant was considered as the readily extractable EPS, representing the LB-EPS. For TB-EPS extraction, the remaining sludge pellet in the centrifuge tube was resuspended in a 100 mM NaCl solution to its original volume of 40 mL. The sludge suspension was then heated to 60 °C in a water-bath for 30 min, after which the mixture was centrifuged at 12,000*g* for 20 min at 4 °C. The collected supernatant was considered as the TB-EPS extraction of the sludge. All supernatant samples were filtered using 0.45 μm acetate cellulose membranes. For each fraction, PS and PN were analyzed using colorimetric methods, resulting in the determination of polysaccharides in loosely bound EPS (PS LB-EPS), proteins in loosely bound EPS (PN LB-EPS), ratio between proteins and polysaccharides in loosely bound EPS (PN/PS LB-EPS), polysaccharides in tightly bound EPS (PS TB-EPS), proteins in tightly bound EPS (PN TB-EPS) and ratio between proteins and polysaccharides in tightly bound EPS (PN/PS TB-EPS). The sum of LB-EPS (PN LB-EPS + PS LB-EPS) and TB-EPS (PN TB-EPS + PS TB-EPS) was also assessed as Total EPS. The PN analysis was performed using a UV/VIS spectrophotometer (DR 500 Hach Lange, Dusseldorf, Germany), following the modified Lowry method with bovine serum albumin (BSA) as the standard. The PS content was determined using the anthrone-sulfuric acid method, employing glucose as the standard [18].

Three-dimensional excitation-emission matrix (3D-EEM) fluorescence was also used to analyze the extracted EPS samples. Fluorescence regional integration, a quantitative technique that integrates the volume below an EEM was applied to analyze EEMs, resulting in the percent fluorescence response (Pi,n) of the organic compounds, as protein-like

substances [19]. The 3D-EEM spectra were collected according to [20]. A luminescence spectrophotometer (Aqualog, Horiba) and the software Origin 8.0 were used to collect and process the spectra from EPS samples, respectively.

2.4. Image acquisition, processing, and analysis

A volume of 10 μL, of a sample collected at the beginning of the aeration phase, was placed on a slide and 50 images were acquired in the upper, middle and bottom of the slide, resulting in a total of 150 images (3 × 50 images per slide). An Olympus BX51 microscope (Olympus, Shinjuku, Japan) at 40 × magnification, coupled to an Olympus DP72 camera (Olympus, Tokyo, Japan), was used for visualization and acquisition. Images were then acquired with cellSens software (Olympus, Shinjuku, Japan) in 1360 × 1024 pixels and 8-bit format. Matlab 9.2 (The Mathworks, Inc., Natick, USA) was used to process all acquired images. Detailed description of these routines can be found elsewhere [14,21]. From the resulting binary images, aggregates and filaments were characterized. Aggregates were divided into 3 size classes according to their equivalent diameter (Deq): small (<25 μm), intermediate (25–250 μm), and large (>250 μm). The parameters obtained from the processed images can be found in the supplementary information (SI, Section 1, Table S1.1). Furthermore, the total filaments length per mixed liquor suspended solids (TL/MLSS) parameter was also assessed, given that it is considered a valuable parameter in QIA.

2.5. Multivariate statistical analysis

In order to extract additional, uncorrelated components (latent vectors), from the original input dataset, relevant to the output parameter(s) model, PLS, a linear multivariate statistical approach is frequently applied [22]. PLS was used to assess EPS fractions and components (Y), namely LB-EPS, PS LB-EPS, PN LB-EPS, TB-EPS, PS TB-EPS, PN TB-EPS, and Total EPS, using 51 parameters (SI, Section 2, Table S2.1). Two different PLS analysis were fed with the acquired data, PLS-1 considering all experimental observations (n = 60, composed the X matrix) and PLS-2 considering each phase as an independent model (n = 15, composed the X matrix). Tables 1 and 2 present the selected variables and variable importance in the projection (VIP) values for each PLS model describing the different EPS types. The first step employed for modeling the EPS was the PLS analysis using the raw dataset containing all QIA variables. The variables were sorted by the highest VIP values, with cross-correlation performed next to eliminate one variable for each pair representing a correlation factor above 0.9. The second step was to perform the PLS analysis again and select the latent variables (LV) with the highest VIP values [15]. After modelling each individual phase, a correlation regression was performed combining the ensemble of the individually obtained results for each phase. For each PLS analysis, the prediction model regression equation, coefficient of determination (R^2), root mean square error of prediction (RMSEP), and residual prediction deviation (RPD) values were determined. The models' limits of applicability (minimum and maximum) for each studied EPS fraction and component were also identified. PLS was performed with Matlab 9.2 software (The MathWorks, Inc. Natick, USA).

3. Results and discussion

3.1. Reactor performance

Data on SBR performance in terms of COD, TIN, and ATZ removal efficiencies can be found in the supplementary material (SI, Section 3, Table S3). Briefly, the obtained results suggest that both organic matter and TIN removal were affected under ATZ exposure, showing a high variability in removal efficiencies. The sudden decrease in COD and N-NH_4^+ in the beginning of each phase can be attributed to ATZ addition causing a temporary shock to the microorganisms due to the sudden change in the concentration and composition of feeding solutions [23] (SI, Section 3, Fig. S3.1). The larger impact on TIN removal efficiency indicates a higher effect on the nitrification, denitrification, and/or assimilation capacity of AS exposed to ATZ (SI, Section 3, Fig. S3.1). The results from ATZ removal efficiency (46.7 %, on average) indicate that microorganisms involved in ATZ biodegradation may prevail in the

Table 1
Selected variables and VIP values for PS and PN LB-EPS, PS and PN TB-EPS, LB-EPS, TB-EPS, and total EPS for the global PLS regression models.

GLOBAL DATA													
PS LB-EPS		PN LB-EPS		PS TB-EPS		PN TB-EPS		LB-EPS		TB-EPS		TOTAL EPS	
Parameters	VIP	Parameters	VIP	Parameters	VIP	Parameters	VIP	Parameters	VIP	Parameters	VIP	Parameters	VIP
Ecc_{int}	1.60	$\%Nb_{int}$	1.43	Deq_{sml}	1.45	$Width_{int}$	1.49	$\%Nb_{int}$	1.44	$Length_{int}$	1.44	$Area/Vol_{int}$	1.43
Deq_{int}	1.36	$LrgC_{sml}$	1.34	$RelArea_{larg}$	1.25	Sol_{larg}	1.48	$Length_{int}$	1.43	$Area/Vol_{larg}$	1.37	$\%Nb_{larg}$	1.35
$Comp_{larg}$	1.27	Sol_{sml}	1.27	$Length_{sml}$	1.24	$\%Nb_{larg}$	1.28	Ecc_{int}	1.38	Sol_{larg}	1.32	Sol_{larg}	1.34
Ext_{sml}	1.15	$Round_{larg}$	1.24	Rob_{sml}	1.22	$RelArea_{larg}$	1.26	FF_{sml}	1.33	$Area_{sml}$	1.29	$Length_{int}$	1.33
$LrgC_{larg}$	1.12	$\%A_{int}$	1.15	$Area/Vol_{int}$	1.15	$Width_{sml}$	1.23	Sol_{int}	1.22	$RelArea_{larg}$	1.19	$Area/Vol_{larg}$	1.24
Rob_{int}	1.10	TL/MLSS	1.14	Rob_{larg}	1.11	$Area/Vol_{int}$	1.11	Per_{sml}	1.19	$Area/Vol_{int}$	1.17	$\%Nb_{int}$	1.21
Nb_{fil}/Vol	1.03	$LrgC_{int}$	1.08	Ext_{int}	1.07	TL/MLSS	1.11	$Area/Vol_{larg}$	1.06	$Length_{sml}$	1.12	FF_{sml}	1.16
$Area_{sml}$	1.01	Per_{sml}	1.06	Sol_{larg}	1.04	Rob_{larg}	1.07	$LrgC_{sml}$	0.98	TL/MLSS	1.11	$RelArea_{int}$	1.02
$Width_{larg}$	1.00	Nb/Vol_{larg}	0.95	FF_{larg}	1.01	$Length_{sml}$	1.00	$RelArea_{int}$	0.95	$\%Nb_{larg}$	1.07	FF_{int}	1.01
TA/Vol	0.98	Ecc_{int}	0.94	$Conv_{int}$	1.00	Nb/Vol_{larg}	0.98	Nb_{fil}/Vol	0.91	Ecc_{larg}	0.99	TL/TA	0.98
$LrgC_{sml}$	0.93	FF_{int}	0.92	TL/MLSS	0.98	$\%Nbi_{int}$	0.92	$Area/Vol_{int}$	0.88	Ext_{sml}	0.92	Ecc_{int}	0.93
$\%Nb_{larg}$	0.93	$\%Nb_{larg}$	0.90	$Area/Vol_{larg}$	0.96	TA/Vol	0.90	Sol_{larg}	0.86	Deq_{larg}	0.81	$LrgC_{sml}$	0.89
$\%A_{int}$	0.92	Nb/Vol_{int}	0.89	$\%Nb_{larg}$	0.91	$Area_{larg}$	0.80	FF_{larg}	0.82	$RelArea_{int}$	0.80	Ecc_{larg}	0.87
Per_{int}	0.90	$Conv_{larg}$	0.86	Ext_{sml}	0.86	FF_{larg}	0.78	$Conv_{larg}$	0.75	Per_{larg}	0.77	Ecc_{sml}	0.86
$RelArea_{larg}$	0.72	Rob_{sml}	0.82	$Length_{int}$	0.83	Per_{larg}	0.73	Rob_{sml}	0.75	Ecc_{larg}	0.71	FF_{larg}	0.69
Rob_{sml}	0.72	$RelArea_{int}$	0.79	Per_{larg}	0.75	FF_{sml}	0.67	TA/Vol	0.73	$Length_{larg}$	0.66	$Conv_{int}$	0.66
Nb/Vol_{int}	0.71	TA/Vol	0.78	Ecc_{int}	0.74	$\%A_{sml}$	0.64	Ecc_{larg}	0.72	Ecc_{int}	0.65	Ecc_{larg}	0.60
Rob_{larg}	0.69	Rob_{larg}	0.66	Ecc_{larg}	0.68	Ecc_{sml}	0.64	$Comp_{larg}$	0.72	FF_{larg}	0.64	$RelArea_{larg}$	0.58
Per_{larg}	0.68	$Width_{sml}$	0.63	$Width_{larg}$	0.64	$LrgC_{sml}$	0.58	$\%Nb_{larg}$	0.60	Ext_{larg}	0.63	$Area_{larg}$	0.50
FF_{larg}	0.59	FF_{larg}	0.63	$Conv_{larg}$	0.62	Rob_{int}	0.52	$Length_{larg}$	0.49	Rob_{sml}	0.58	Per_{larg}	0.43

Table 2
Selected variables and VIP values for PS and PN LB-EPS, PS and PN TB-EPS, LB-EPS, TB-EPS, and total EPS for the PLS regressions for phases I-IV.

PS LB-EPS

Phase I		Phase II		Phase III		Phase IV	
Parameters	VIP	Parameters	VIP	Parameters	VIP	Parameters	VIP
$LrgC_{larg}$	1.66	Rob_{sml}	1.48	Ecc_{sml}	1.36	Ecc_{larg}	1.60
$Comp_{larg}$	1.16	TL/Vol	1.42	$Width_{larg}$	1.10	$Area/Vol_{int}$	1.28
TNb/Vol	1.11	Nb/Vol_{larg}	1.29	$\%A_{larg}$	1.07	$Conv_{int}$	1.09
$Length_{int}$	1.00	$LrgC_{int}$	0.95	$\%A_{int}$	1.07	Rob_{larg}	1.02
$\%A_{int}$	0.88	$Length_{larg}$	0.93	Sol_{larg}	1.05	TL/TA	1.01
Nb/Vol_{int}	0.86	Nb_{thn}/Vol	0.85	$RelArea_{larg}$	0.90	$LrgC_{int}$	0.91
$Area/Vol_{int}$	0.85	TL/TA	0.72	$LrgC_{larg}$	0.89	$RelArea_{int}$	0.72
$Area/Vol_{larg}$	0.76	FF_{sml}	0.64	Ecc_{int}	0.87	$Conv_{larg}$	0.71
Ecc_{larg}	0.71	$RelArea_{int}$	0.62	Rob_{larg}	0.79	TA/Vol	0.70
$Area_{int}$	0.58	Deq_{larg}	0.53	Per_{larg}	0.75	$LrgC_{larg}$	0.49

PN LB-EPS

Phase I		**Phase II**		**Phase III**		**Phase IV**	
Parameters	VIP	Parameters	VIP	Parameters	VIP	Parameters	VIP
Ecc_{int}	1.89	$LrgC_{int}$	1.46	Sol_{sml}	1.38	FF_{sml}	1.47
Ecc_{larg}	1.47	$RelArea_{int}$	1.23	$LrgC_{larg}$	1.37	Ecc_{larg}	1.05
$RelArea_{larg}$	0.94	Deq_{larg}	1.20	Ecc_{int}	1.28	FF_{larg}	1.05
Deq_{larg}	0.92	Rob_{sml}	1.11	$\%Nb_{larg}$	0.92	$Area/Vol_{larg}$	1.04
$RelArea_{int}$	0.87	$LrgC_{sml}$	0.91	$RelArea_{larg}$	0.87	Nb/Vol_{int}	0.99
Per_{larg}	0.73	$Length_{int}$	0.90	$Conv_{larg}$	0.86	Nb_{fil}/Vol	0.99
$Conv_{larg}$	0.69	Rob_{int}	0.87	Per_{larg}	0.80	Ext_{larg}	0.98
$\%A_{int}$	0.58	Nb/Vol_{larg}	0.79	$Length_{larg}$	0.76	Per_{larg}	0.85
$Area/Vol_{sml}$	0.58	$Conv_{larg}$	0.67	Ext_{int}	0.73	$Conv_{int}$	0.75
Rob_{larg}	0.27	TA/Vol	0.47	$Area_{larg}$	0.70	$Width_{larg}$	0.62

PS TB-EPS

Phase I		**Phase II**		**Phase III**		**Phase IV**	
Parameters	VIP	Parameters	VIP	Parameters	VIP	Parameters	VIP
$\%Nb_{larg}$	1.48	Ecc_{sml}	1.43	$Conv_{larg}$	1.62	FF_{larg}	1.31
TL/MLSS	1.47	$Width_{sml}$	1.26	$Conv_{int}$	1.41	Per_{larg}	1.29
Ecc_{larg}	1.40	$Width_{larg}$	1.11	$Round_{sml}$	1.10	Deq_{sml}	1.24
Rob_{larg}	1.18	Nb/Vol_{larg}	1.10	$\%A_{larg}$	0.97	$\%Nb_{larg}$	1.14
$Area_{sml}$	1.13	Sol_{sml}	1.04	$\%A_{int}$	0.94	$\%Nb_{int}$	1.00
$RelArea_{int}$	0.53	$\%A_{int}$	0.95	Rob_{sml}	0.88	Nb/Vol_{int}	0.87
$Conv_{sml}$	0.51	$\%A_{larg}$	0.88	Per_{larg}	0.76	Ecc_{sml}	0.82
TA/Vol	0.50	Ecc_{larg}	0.68	Ext_{int}	0.63	$Length_{sml}$	0.68
$Width_{sml}$	0.45	$LrgC_{int}$	0.67	$Area_{larg}$	0.56	TA/Vol	0.66
$Width_{int}$	0.16	Per_{larg}	0.50	$Length_{larg}$	0.54	TL/TA	0.65

PN TB-EPS

Phase I		**Phase II**		**Phase III**		**Phase IV**	
Parameters	VIP	Parameters	VIP	Parameters	VIP	Parameters	VIP
$Width_{int}$	1.61	$Width_{sml}$	1.46	$Conv_{int}$	1.70	Nb/Vol_{int}	1.34
$RelArea_{int}$	1.57	Nb/Vol_{larg}	1.18	$Round_{sml}$	1.33	$Length_{sml}$	1.27
TL/MLSS	1.19	$Width_{larg}$	1.13	$LrgC_{sml}$	1.06	$\%Nb_{sml}$	1.15
$\%A_{larg}$	0.94	$Comp_{sml}$	1.10	Ecc_{larg}	0.97	Nb_{fil}/Vol	1.03
TL/TA	0.89	FF_{sml}	1.03	Rob_{sml}	0.96	Deq_{sml}	1.02
$LrgC_{sml}$	0.81	Nb_{thn}/Vol	0.88	TA/Vol	0.86	FF_{larg}	0.96
$Conv_{sml}$	0.70	$Conv_{larg}$	0.84	$Area/Vol_{larg}$	0.81	$\%Nb_{larg}$	0.80
$\%Nb_{larg}$	0.54	Sol_{sml}	0.78	$Area_{larg}$	0.66	$Conv_{larg}$	0.78
Rob_{larg}	0.48	$Comp_{int}$	0.74	$Conv_{larg}$	0.59	$Area/Vol_{larg}$	0.72
Nb/Vol_{larg}	0.48	TL/TA	0.54	Per_{larg}	0.42	$\%A_{larg}$	0.68

LB-EPS

Phase I		**Phase II**		**Phase III**		**Phase IV**	
Parameters	VIP	Parameters	VIP	Parameters	VIP	Parameters	VIP
Ecc_{int}	1.63	$LrgC_{int}$	1.39	Ecc_{int}	1.55	FF_{sml}	1.38
$Area_{sml}$	1.26	$Comp_{int}$	1.23	$Conv_{larg}$	1.09	$Area_{larg}$	1.36
$Area_{larg}$	1.21	Rob_{sml}	1.02	Sol_{larg}	1.09	Nb_{fil}/Vol	1.25
Rob_{sml}	0.99	Rob_{int}	1.01	Sol_{sml}	1.07	$Width_{larg}$	1.22
$RelArea_{larg}$	0.99	Deq_{larg}	0.98	Ext_{int}	1.06	$Area_{int}$	0.94
Ecc_{larg}	0.80	Nb_{larg}	0.98	$Length_{larg}$	0.96	Ecc_{larg}	0.93
$Conv_{larg}$	0.75	$Conv_{larg}$	0.94	$Area_{larg}$	0.87	Rob_{larg}	0.85

(*continued on next page*)

Table 2 (*continued*)

PS LB-EPS							
Phase I		Phase II		Phase III		Phase IV	
Parameters	VIP	Parameters	VIP	Parameters	VIP	Parameters	VIP
$Comp_{larg}$	0.68	$Length_{sml}$	0.92	$LrgC_{larg}$	0.75	TL/TA	0.58
$LrgC_{sml}$	0.64	TA/Vol	0.73	Ecc_{sml}	0.67	TL/MLSS	0.51
Rob_{larg}	0.54	$LrgC_{sml}$	0.54	$Width_{sml}$	0.50	Ext_{larg}	0.35

TB-EPS

Phase I		**Phase II**		**Phase III**		**Phase IV**	
Parameters	VIP	Parameters	VIP	Parameters	VIP	Parameters	VIP
$RelArea_{int}$	1.37	$Width_{sml}$	1.59	$Conv_{int}$	1.65	FF_{int}	1.25
Ecc_{larg}	1.35	$Width_{larg}$	1.41	$Round_{sml}$	1.14	$\%Nb_{sml}$	1.23
$Area_{larg}$	1.29	Ecc_{sml}	1.20	Ext_{int}	1.10	Nb_{fil}/Vol	1.21
Rob_{larg}	1.09	$LrgC_{sml}$	0.99	$\%A_{larg}$	0.91	Deq_{sml}	1.16
$Comp_{larg}$	1.03	Ext_{sml}	0.97	$LrgC_{larg}$	0.90	FF_{sml}	1.16
TA/Vol	0.98	Nb_{int}/Vol	0.93	$Conv_{larg}$	0.88	$Length_{sml}$	0.84
TL/MLSS	0.77	Rob_{larg}	0.69	$LrgC_{sml}$	0.85	Per_{int}	0.82
Nb/Vol_{larg}	0.59	Per_{sml}	0.59	Rob_{sml}	0.84	$\%Nb_{larg}$	0.76
$Width_{int}$	0.53	$Conv_{larg}$	0.53	$Area_{larg}$	0.71	Ecc_{sml}	0.72
$Conv_{sml}$	0.46	$LrgC_{larg}$	0.39	TA/Vol	0.66	$\%A_{larg}$	0.52

Total EPS

Phase I		**Phase II**		**Phase III**		**Phase IV**	
Parameters	VIP	Parameters	VIP	Parameters	VIP	Parameters	VIP
Nb_{int}/Vol	1.74	Nb_{int}/Vol	1.59	$RelArea_{larg}$	1.58	FF_{larg}	1.31
$Area/Vol_{larg}$	1.19	$Round_{sml}$	1.48	$\%A_{int}$	1.11	Nb/Vol_{int}	1.26
Rob_{larg}	1.10	Ecc_{int}	1.36	Ecc_{int}	1.08	Ext_{larg}	1.26
$Width_{larg}$	1.07	$Width_{sml}$	1.01	$\%A_{larg}$	1.07	$Comp_{larg}$	1.23
$\%A_{int}$	1.01	Ecc_{larg}	0.87	$Round_{sml}$	1.07	$Conv_{int}$	1.16
$LrgC_{sml}$	0.80	$LrgC_{int}$	0.82	$Area_{larg}$	1.04	$Area_{larg}$	0.94
$\%Nb_{larg}$	0.76	$LrgC_{sml}$	0.58	Sol_{larg}	0.85	Ecc_{larg}	0.69
Per_{larg}	0.73	$Width_{larg}$	0.57	Nb/Vol_{larg}	0.61	FF_{int}	0.67
Nb/Vol_{larg}	0.68	$Round_{int}$	0.45	Rob_{sml}	0.61	$Area_{int}$	0.60
$Conv_{sml}$	0.34	Per_{larg}	0.32	$Comp_{sml}$	0.52	Nb/Vol_{larg}	0.31

system (SI, Section 3, Fig. S3.1). Previous studies have reported ATZ removal efficiencies above 47 % [23], and of 51 % [24], which aligns with the results obtained in the present work.

3.2. EPS fractions and components

LB-EPS and TB-EPS in the biomass were monitored throughout the experimental phases (Fig. 1). It became evident that ATZ exposure affected the EPS fractions. LB-EPS increased from phase I to phase II and from phase III to phase IV, while TB-EPS increased from phase I to phase IV (Fig. 1a). The presence of toxic substances is known to intensify EPS production, reducing damage to microbial [25–27]. Additionally, LB- and TB-EPS might interact differently with herbicide compounds [28]. The PN/PS ratio has been used as an indicator of EPS fractions' relative hydrophobicity [29,30], with all PN/PS ratio fractions exhibiting an increase following the addition of ATZ (Fig. 1a; SI, Section 3, Table S3.2). Consequently, significant differences ($p < 0.05$) in the PN/PS EPS ratio were observed between phase I and phases II–IV (SI, Section 3, Table S3.2), indicating an increased hydrophobicity of the sludge surface due to changes in the PN content. Our findings revealed the substantial impact of elevated ATZ concentrations on microbial activity and EPS composition, particularly LB-EPS. Microscopic analysis, outlined in the SI (Section 3, Fig. S3.2), unveiled noticeable alterations in microbial structure. Notably, exposure to ATZ led to the suppression of filamentous bacteria and an increase in the prevalence of large aggregates. These observed changes likely contributed to the variations in LB-EPS values. Consequently, during phase IV, the production of PS resulted in a reduction in the PN/PS ratio of LB-EPS. Thus, the adaptability of microorganisms to toxic compounds likely facilitated increased EPS release, consequently altering its composition [31], potentially affecting the stability and structure of biomass aggregates [32]. Moreover, the findings presented in this study align with those previously mentioned.

Fig. 1b, c shows the LB-EPS and TB-EPS components. Oxidative stress is one of the reported adverse effects of ATZ in microorganisms, being also observed significant changes in their metabolism in response to ATZ exposure. Existing literature indicates that amino acids serve to protect against oxidative stress by enhancing and stabilizing redox enzyme [33], and may additionally function as a defensive mechanism against protein oxidation [34]. Moreover, EPS has been identified as a protective mechanism to alleviate toxicity, such as oxidative stress, triggered by the concurrent presence of perfluorooctanoic acid and polystyrene microplastics [35]. The overall results for LB-EPS and TB-EPS components suggest that the addition of ATZ favored the increase of hydrophobic regions in EPS [29,36,37] since PN/PS ratio results were more remarkable in the phases with ATZ addition than in phase I. It was further calculated that the percent fluorescence response of protein-like substances remained almost stable for phases I, II and IV, increasing during phase III for LB-EPS and decreasing for TB-EPS (SI, Section 3, Table S3.3). In the presence of ATZ, it is possible to observe that the percent fluorescence response values of protein-like substances, only for TB-EPS, were consistently below the values obtained without ATZ, suggesting that protein-like substances were quenched in the presence of ATZ. Moreover, the results obtained for LB-EPS indicate that this fraction of the biopolymers did not interact with ATZ, which explains the increase in the percent fluorescence response in phase III. Indeed, PN might dominate the interaction between ATZ and EPS due to the presence of more potential adsorption sites for ATZ adsorption than PS. Furthermore, PN contains more functional groups than PS, such as aromatic amino acid substances, favoring the formation of an ATZ-EPS complex [38], thus giving a protective response of bacteria under ATZ

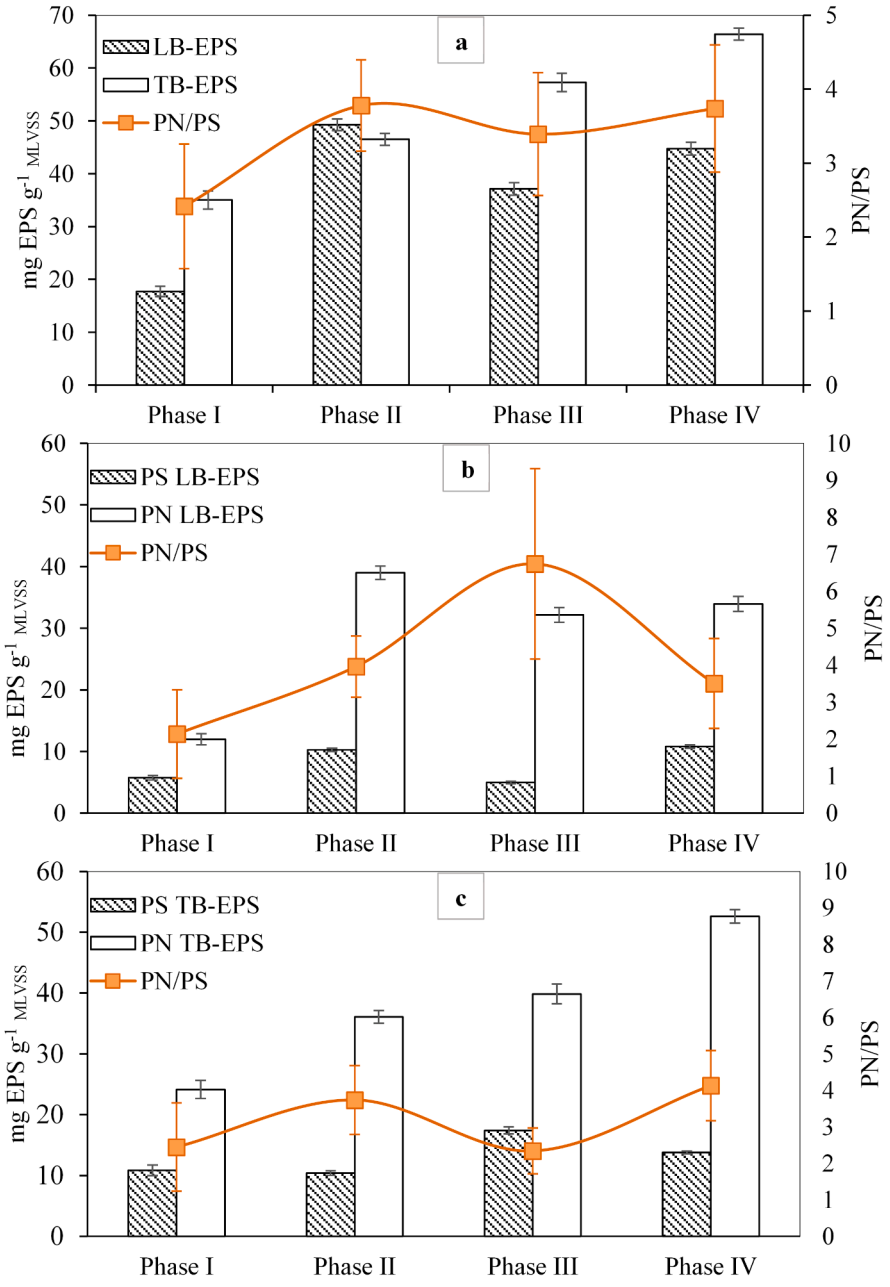

Fig. 1. EPS fractions and components during the SBR operation. LB-EPS, TB-EPS and total PN/PS ratio (a), PS, PN, and PN/PS ratio of the LB-EPS fraction (b), PS, PN, and PN/PS ratio of the TB-EPS fraction (c).

exposure.

3.3. Settling ability and quantitative image analysis

The settling ability and morphological changes of AS during ATZ exposure were also assessed (Fig. 2). The TL/MLSS, a valuable parameter determining the relationship between the presence of free filamentous bacteria and aggregates [21], decreased mainly in the first two experimental phases, consistently falling below the threshold value of 10,000 mm mg^{-1} MLSS reported by [39]. This indicates the absence of possible filamentous bulking phenomena (Fig. 2a). Additionally, the settling ability of AS evolved throughout the different phases, with SVI varying from 167 to 68 mL g^{-1} MLSS (Fig. 2a). The sludge exhibited poor settling ability when SVI values were higher than or close to 150 mL g^{-1} MLSS, observed mainly during phase I and until the middle of phase II. This result suggests that factors beyond filamentous content influenced the sludge settling properties [40]. Interestingly, data from phase II demonstrate a positive correlation between LB-EPS and SVI results (SI, Section 3, Table S3.4). Considering the significance of EPS in the formation of sludge flocs, it is essential to recognize that an overabundance of LB-EPS may impair cell attachment and weaken the floc structure. This phenomenon often leads to suboptimal sludge-water separation [12]. The increase in LB-EPS content observed during phase II probably disrupted the microenvironment of floccular sludge, intensifying the degradation of the sludge floc structure and reducing the settling capacity of AS. However, as the phases progressed, SVI values decreased, reaching the lowest value of 68 mL g^{-1} MLSS during phase IV.

The aggregates area distribution, presented in Fig. 2b, reveals a significant presence of intermediate aggregates during phase I ($\%A_{int}$ of 81.2 ± 4.7 %, on average). In phase II, the behavior was opposite for large and intermediate aggregates. While $\%A_{int}$ decreased to 50.6 ± 1.7

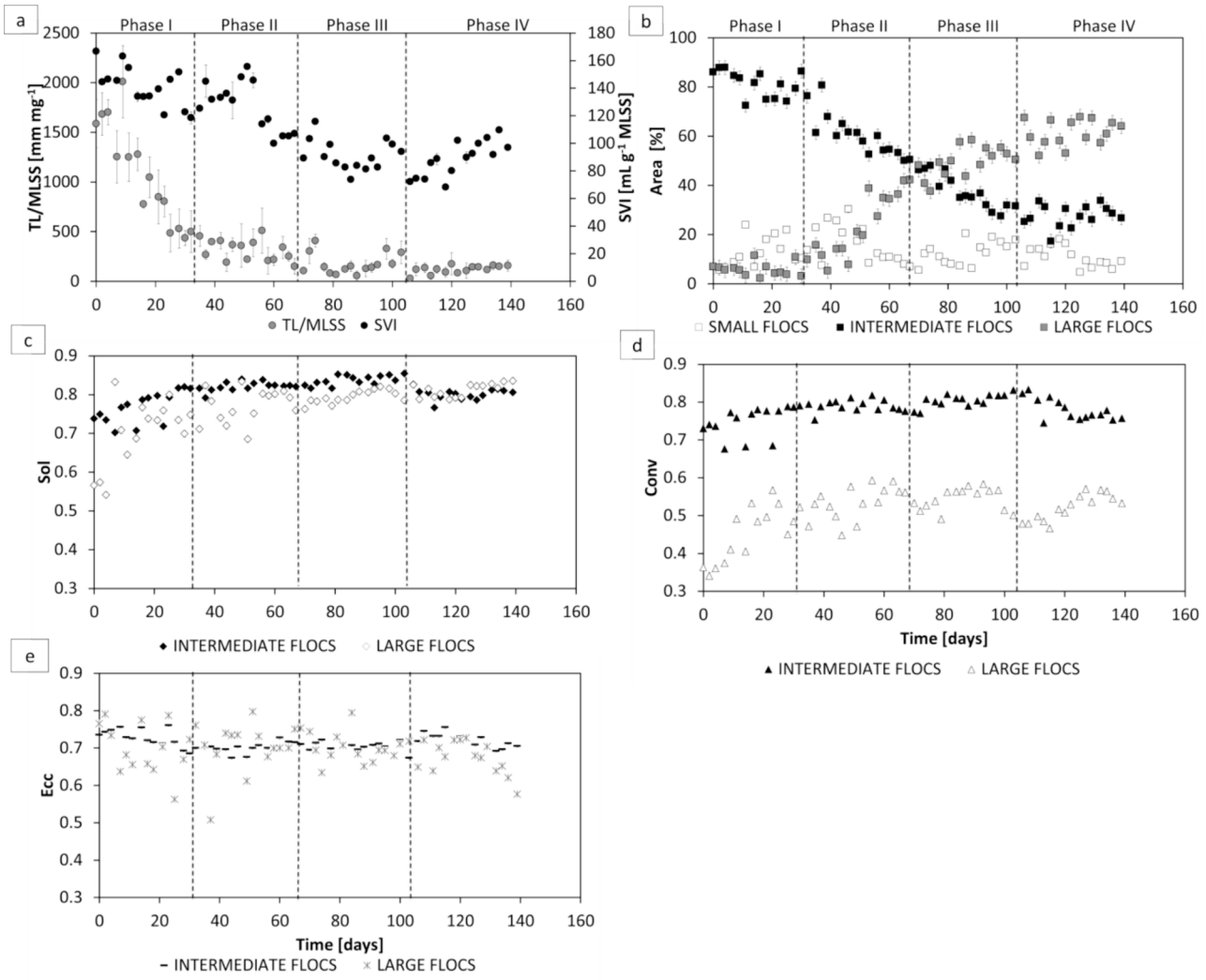

Fig. 2. AS profile during SBR operation. TL/MLSS and SVI (a), Area percentage of aggregates, $\%A_{sml}$, $\%A_{int}$, and $\%A_{larg}$ (b), Solidity of aggregates, Sol_{int} and Sol_{larg} (c), Convexity of aggregates, $Conv_{int}$ and $Conv_{larg}$ (d), Eccentricity of aggregates, Ecc_{int} and Ecc_{larg} (e).

%, the $\%A_{larg}$ increased to 42.3 ± 3.8 %. From the beginning of phase III (day 74) until the end of phase IV, there was a notable presence of large aggregates ($\%A_{larg}$ from 48.2 ± 5.2 % to 64.0 ± 5.8 %) especially in phases III and IV exposed to higher ATZ concentrations. This rise in large aggregates seems to be closely related to the increase in TB-EPS and total EPS production. The evolution of the aggregates structure across all phases can be observed in the supplementary information (SI, Section 3, Fig. 3.2).

Furthermore, aggregates were morphologically characterized based on solidity (Sol, Fig. 2c), convexity (Conv, Fig. 2d), and eccentricity (Ecc, Fig. 2e). In general, intermediate aggregates exhibited compact and elongated structures with regular boundaries (high Sol, Ecc, and Conv values, respectively) across all phases. On the other hand, large aggregates became more compact (Sol values increased from 0.57 to 0.84), and their boundaries became smoother within phase I, though they could still be considered irregular (low Conv) across all phases (Fig. 2c, d). As for the intermediate aggregates, large aggregates presented somewhat elongated structures, though with increased variability (Fig. 2e). The results obtained allowed us to infer a positive impact of the EPS changes across the different phases on the AS settling ability, sludge structure, and morphology. This research aligns with previous studies demonstrating the influence of AS aggregates' surface chemical properties, such as different EPS fractions and components (PS, PN, LB-EPS, TB-EPS, and PN/PS ratios), on the sludge settling ability [11,40,41].

3.4. Variable reduction and VIP

In this work, PLS was used to assess PS and PN LB-EPS, PS and PN TB-EPS, LB-EPS, TB-EPS and total EPS.

In PLS-1, the primary variables (VIP > 0.80) used for modeling all EPS forms are related to morphological descriptors, which is evident from the consistently high VIP values across all PLS models (PS and PN LB-EPS, PS and PN TB-EPS, LB-EPS, TB-EPS, and total EPS), as presented in Table 1. Following the morphological descriptors, the aggregates content descriptor constitutes the second most influential group contributing to the PLS models, encompassing 3–5 variables. Interestingly, the percentage of aggregates per class (%Nb) significantly influenced all PLS models with VIP values greater than 0.90. Specifically, for PN LB-EPS and LB-EPS, the intermediate class %Nb had the highest contribution to the model with VIP values of 1.43 and 1.44, respectively. Regarding the descriptor group of filamentous bacteria, the variable TL/MLSS was the most impactful in building the PLS regression models for PN LB-EPS, PS TB-EPS, PN TB-EPS, and TB-EPS. In contrast, for PS LB-EPS and LB-EPS, the number of filaments per volume (Nbfil/Vol) played a more significant role, presenting VIP values of 1.03 and 1.44, respectively. Moreover, TL/TA, with a VIP value of 0.98, emerged as more significant in the total EPS PLS model.

Regarding PLS-2, the role of different descriptor groups for EPS assessment can be observed in Table 2. The morphological characteristics and aggregates content descriptor groups predominated across all PLS models, contributing with a higher number of variables with VIP > 0.80. The filamentous bacteria content descriptor group appeared in 9 out of 28 PLS models for EPS content assessment, contributing solely with up to 2 variables per model with VIP > 0.80. For the LB-EPS fraction, the aggregates morphological descriptor group accounted for 4 variables in phase I, 5 variables in phase II, 5 variables in phase III, and 3 variables in phase IV, with VIP > 0.80. Additionally, 2 variables from the aggregates content descriptor group with VIP > 0.80 appeared in the PLS models for phases I and IV, and 1 variable for phases II and III. Only 1 variable from the aggregates size descriptor group presented a VIP > 0.80 for phases II, III, and IV, and 1 variable from the filamentous bacteria content descriptor group for phase IV. Concerning the PS LB-EPS component, and for all phases, the variables from the aggregates morphological and content descriptor groups were the most relevant. For phases I, II, and III, a single variable from the aggregates size descriptor group presented a VIP > 0.8, whereas the filamentous bacteria content descriptor group also contributed to the models with VIP > 0.8 for phases II and IV. For the PN LB-EPS models, the variables that contributed the most were again from the aggregates morphological descriptor group (4 to 5 variables) for all phases. The aggregates content descriptor group accounted for only 1 and 2 variables with VIP > 0.8 for phase III and IV, respectively. On the other hand, a single variable from the aggregates size descriptor group presented a VIP > 0.8 for phase I, 2 variables for phase II, and 1 variable for phase III, whereas the filamentous bacteria content descriptor group accounted for a single variable with VIP > 0.8 for phase IV.

For the TB-EPS fraction, variables with a VIP > 0.8 were obtained from both the aggregates morphological and content descriptor groups, influencing the models for all phases. Additionally, the aggregates size descriptor group influenced the PLS models for phases II and IV, and the filamentous bacteria content descriptor group for phase IV. Both the aggregates morphological and content descriptor groups presented at least 2 variables with a VIP > 0.8 for PS TB-EPS across all phases. Additionally, 2 variables from the aggregates size descriptor group presented a VIP > 0.8 for phases II and IV. Interestingly, TL/MLSS, a variable from the filamentous bacteria content descriptor group, presented a VIP value of 1.47, largely contributing to the PS TB-EPS PLS model of phase I. Moreover, three out of the four descriptor groups (aggregates morphology, aggregates content, and filamentous bacteria content) impacted the PLS models for PN TB-EPS. In contrast, the aggregates size descriptor group only contributed for phases II and IV with 2 variables presenting a VIP > 0.8.

Regarding the total EPS, a single variable from the filamentous bacteria content descriptor group presented the highest VIP values of 1.74 and 1.59 for phases I and II, respectively. On the other hand, the aggregates morphological descriptor group was the most suited for assessing total EPS, with the higher number of variables presenting a VIP > 0.8 across all phases. Furthermore, the aggregates size descriptor group also influenced the prediction of total EPS, mainly in phases I and II, whereas the aggregates content descriptor group impacted phases I, III, and IV.

So far, it is well-established that EPS play a crucial role in the formation of flocs (aggregates), facilitating hydrophobic interactions and binding floc constituents, which may be associated with their morphological characteristics [42]. Additionally, higher EPS quantities have been linked to larger flocs [43], and EPS are known to participate in the granulation processes, contributing to the maintenance of granule structure, indicating their involvement in changes in aggregates' size [44]. Furthermore, it has been recognized that specific EPS components, rather than just the overall amount of EPS, play a significant role in determining differences in sludge morphology [44–46].

PN has been reported to influence microbial cell aggregation and the alteration of hydrophobic interactions between microbial cells [47]. In line with this [44] identified PN, particularly β-sheets, as critical factors in causing changes in sludge size during the sludge granulation process. Additionally, hydrophobicity, often measured by the PN/PS ratio, has also been observed to impact the aggregation process, leading to shifts in bioaggregates' morphology [44].

In line with these findings, Wang et al. (2021) observed that after TB-EPS extraction, the free energy (ΔG) of sludge samples increased, indicating a significant reduction in sludge hydrophobicity and an increase in the adsorption capacity between sludge and water. The authors attributed this effect to TB-EPS, which played a crucial role in sludge granulation by enhancing its adsorption on sludge cells and promoting cell aggregation [48].

Taking the above into consideration, it is evident that the different EPS fractions and components possess distinct physical and chemical properties, leading to various effects on sludge properties and influencing the morphology of the aggregates [48]. Consequently, this fact can elucidate the prevalence of aggregates morphology descriptors with higher VIP values (Tables 1 and 2) in assessing PS, PN, LB-EPS, TB-EPS, and total EPS content. Additionally, the present results suggest that a higher concentration of ATZ led to an increase in EPS content, primarily governed by large aggregates during phases III and IV. Furthermore, the assessment of EPS fractions and components mainly relied on large and intermediate morphological descriptors, which represented the key variables.

3.5. EPS assessment

The regression equation, LV, RMSEP, and RPD values are presented for the global (training + validation) dataset, while the R^2 values are presented separately for the global, training and validation datasets (Table 3). An RPD value, indicating the ratio between the standard deviation of the observed values and RMSEP, larger than 3 is recommended for screening purposes [17,49].

For PLS-1, the obtained PLS models did not fit well with the EPS contents (matrix Y). The RPD values for all global models were consistently below 3, indicating that the PLS regression models obtained were not effective in assessing the EPS fractions and components. Additionally, low R^2 values were achieved, ranging from 0.42 for PS LB-EPS to 0.74 for total EPS (Table 3).

In contrast, PLS-2 proved to be more successful in assessing the EPS fractions and components, as shown in Table 3. Regarding LB-EPS fraction, the RMSEP varied from1.9 mg $g_{ML\ VSS}^{-1}$ to 6.4 mg $g_{ML\ VSS}^{-1}$, representing from 3.85 % to 17.30 % of the observed values range. For the PS LB-EPS component, the RMSEP ranged from 0.5 mg $g_{ML\ VSS}^{-1}$ to 1.3 mg $g_{ML\ VSS}^{-1}$, corresponding from 10.21 % to 22.86 % of the observed values range, respectively. For the PN LB-EPS component, the RMSEP varied from 2.0 mg $g_{ML\ VSS}^{-1}$ to 3.0 mg $g_{ML\ VSS}^{-1}$, representing from 5.17 % to 8.71 % of the observed values range. Similarly, for the TB-EPS fraction, the RMSEP ranged from 2.2 mg $g_{ML\ VSS}^{-1}$ to 7.3 mg $g_{ML\ VSS}^{-1}$, representing from 4.76 % to 20.79 % of the observed values range. Additionally, the RMSEP for PS TB-EPS varied from 1.1 mg $g_{ML\ VSS}^{-1}$ to 1.9 mg $g_{ML\ VSS}^{-1}$, corresponding from 10.86 % to 18.90 % of the observed values range, and for PN TB-EPS, RMSEP ranged from 3.2 mg $g_{ML\ VSS}^{-1}$ to 3.5 mg $g_{ML\ VSS}^{-1}$, corresponding from 6.14 % to 15.50 % of the observed values range. Regarding total EPS, RMSEP values varied from 5.63 mg $g_{ML\ VSS}^{-1}$ to slightly above 10 mg $g_{ML\ VSS}^{-1}$, corresponding from 10.68 % to 9.54 % of the observed values range. In general, the EPS fractions and components presented RPD values above 3 (Table 3) for the global set (training + validation), with exceptions for LB-EPS phase III, PS LB-EPS phase I, and TB-EPS phase I (RPD of 3.0). As for the R^2 values, good prediction abilities (above 0.9) were obtained for the assessment of the EPS fractions and components (Table 3), except for PS LB-EPS phase I (R^2 of 0.86, Table 3).

Finally, Fig. 3 presents the data combining the ensemble of

Table 3
Regression equation, LV, R^2, RMSEP and RPD values for each studied EPS fraction and component (glb – global, trn – training set, and val – validation set, Min – minimum value, Max – maximum value).

Matrix (Y)	PLS	Phase	LV	Regression Equation glb	R^2glb	R^2trn	R^2val	RMSEP	RPD	Min	Max
PS LB-EPS	PLS-1	global	10	Y = 0.69 x + 3.00	0.42	0.75	0.11	4.1	1.2	1.10	20.32
	PLS-2	I	5	Y = 0.99 x + 0.74	0.86	0.97	0.89	1.3	3.0	1.10	14.73
		II	5	Y = 1.01 x – 0.17	0.96	0.98	0.95	0.7	5.1	2.85	15.00
		III	5	Y = 1.00 x – 0.10	0.96	0.98	0.93	0.5	4.9	1.18	10.39
		IV	5	Y = 0.93 x + 0.32	0.92	0.91	0.96	1.6	3.5	2.98	20.32
PN LB-EPS	PLS-1	global	10	Y = 0.81 x + 6.45	0.56	0.66	0.58	12.4	1.4	0.69	58.36
	PLS-2	I	5	Y = 1.00 x + 0.00	0.92	0.96	0.86	2.6	3.5	0.69	31.41
		II	5	Y = 0.95 x + 2.00	0.96	0.98	0.90	2.0	5.5	18.2	54.94
		III	5	Y = 0.96 x + 0.50	0.97	0.99	0.97	2.8	6.1	9.11	58.36
		IV	5	Y = 1.00 x – 0.01	0.96	0.98	0.93	3.0	5.1	14.55	56.04
PS TB-EPS	PLS-1	global	10	Y = 0.80 x + 2.54	0.51	0.78	0.24	6.0	1.2	2.17	38.12
	PLS-2	I	5	Y = 1.00 x + 0.80	0.93	0.99	0.95	1.9	3.3	2.17	22.01
		II	5	Y = 1.00 x + 0.01	0.95	0.96	0.92	1.1	4.5	5.25	22.60
		III	5	Y = 1.00 x + 0.54	0.96	0.98	0.95	1.9	4.8	9.93	38.12
		IV	5	Y = 1.01 x – 0.41	0.93	0.96	0.93	1.9	3.8	5.66	27.04
PN TB-EPS	PLS-1	global	9	Y = 0.73 x + 10.12	0.58	0.66	0.53	13.1	1.4	3.47	83.49
	PLS-2	I	5	Y = 0.97 x + 0.67	0.95	0.94	0.97	3.7	4.6	3.47	50.60
		II	5	Y = 0.98 x – 0.21	0.91	0.96	0.79	3.7	3.2	16.99	52.64
		III	5	Y = 0.97 x – 0.57	0.95	0.98	0.91	4.5	4.2	14.7	71.85
		IV	5	Y = 0.94 x + 3.40	0.97	0.99	0.95	3.2	6.1	25.25	83.49
LB-EPS	PLS-1	global	9	Y = 0.95 x + 2.06	0.52	0.80	0.43	18.5	1.1	1.79	73.83
	PLS-2	I	5	Y = 1.03 x – 0.62	0.97	0.99	0.94	2.0	6.1	1.79	46.14
		II	5	Y = 0.99 x + 1.33	0.98	1.00	0.94	1.9	7.4	21.05	69.94
		III	5	Y = 1.01 x + 0.83	0.90	0.94	0.91	6.4	3.0	10.48	66.28
		IV	5	Y = 1.01 x + 1.31	0.94	0.98	0.94	5.4	3.7	18.92	73.83
TB-EPS	PLS-1	global	10	Y = 0.79 x + 10.22	0.63	0.74	0.54	16.3	1.6	5.78	109.97
	PLS-2	I	5	Y = 0.97 x + 2.94	0.90	0.80	0.99	7.3	3.0	5.78	72.61
		II	5	Y = 1.01 x + 0.00	0.98	0.99	0.96	2.2	7.4	22.24	71.63
		III	5	Y = 0.99 x + 1.15	0.97	0.98	0.93	4.3	6.4	26.41	109.97
		IV	5	Y = 0.99 x – 1.06	0.93	0.98	0.71	7.2	3.6	32.20	109.69
Total EPS	PLS-1	global	10	Y = 1.00 x – 1.24	0.74	0.86	0.72	19.8	1.7	23.36	154.78
	PLS-2	I	5	Y = 1.00 x – 0.32	0.93	0.94	0.94	5.6	3.9	23.36	95.60
		II	5	Y = 0.99 x + 1.01	0.92	0.93	0.91	6.1	3.4	55.1	141.57
		III	5	Y = 0.99 x + 2.19	0.94	0.97	0.88	7.3	4.1	48.73	141.68
		IV	5	Y = 0.91 x + 5.99	0.90	0.96	0.86	10.6	3.1	60.34	154.78

individually obtained results for each phase. The results demonstrate that modeling each phase individually proved to be the most effective strategy in this case (R^2 higher than 0.94). In summary, the implemented strategy, considering the characteristics inherent to each phase, can produce satisfactory PLS models with a remarkably high level of accuracy for EPS prediction, and considerably better than the PLS models considering the whole global data [50]. The present results highlight the significance of conducting independent analyses on data gathered from each phase. Consequently, employing multiple PLS models to predict specific features in a data-variable system can lead to more precise models [51,52].

4. Conclusion

This study has demonstrated that exposure to ATZ hampers both organic matter and TIN, leading to significant variations in removal efficiencies. Notably, the ATZ removal efficiency increased progressively from phase II to phases III and IV, indicating the prevalence of ATZ-degrading microorganisms. Moreover, EPS results indicated a potential interaction between TB-EPS and ATZ. The application of both QIA and chemometrics allowed for the assessment of EPS fractions and components. It was found that employing individual PLS models for each experimental phase was the most effective strategy in successfully assessing EPS content, yielding coefficients of determination (R^2) above 0.86. Finally, this research has unveiled that using QIA parameters to evaluate EPS fractions and components is an environmentally friendly method that reduces the reliance on chemicals, saves time, and holds promise as a complementary monitoring approach in the future. The obtained results offer valuable new insights, particularly from an operational standpoint, into AS monitoring when exposed to ATZ. This contribution will aid in the timely evaluation of EPS fractions and components, specifically in the presence of environmentally relevant concentrations of ATZ. As a result, it is anticipated that this methodology could be applied to monitor full-scale systems in the presence of emerging compounds in the near future.

CRediT authorship contribution statement

Antonio Melo: Writing – original draft, Investigation, Formal analysis. **Joana Costa:** Investigation, Formal analysis. **Cristina Quintelas:** Writing – review & editing, Investigation, Formal analysis. **António L. Amaral:** Writing – review & editing. **Eugénio C. Ferreira:** Writing – review & editing, Supervision, Funding acquisition. **Daniela P. Mesquita:** Conceptualization, Supervision, Writing – review & editing.

Declaration of competing interest

The authors declare that they have no known competing financial interests or personal relationships that could have appeared to influence the work reported in this paper.

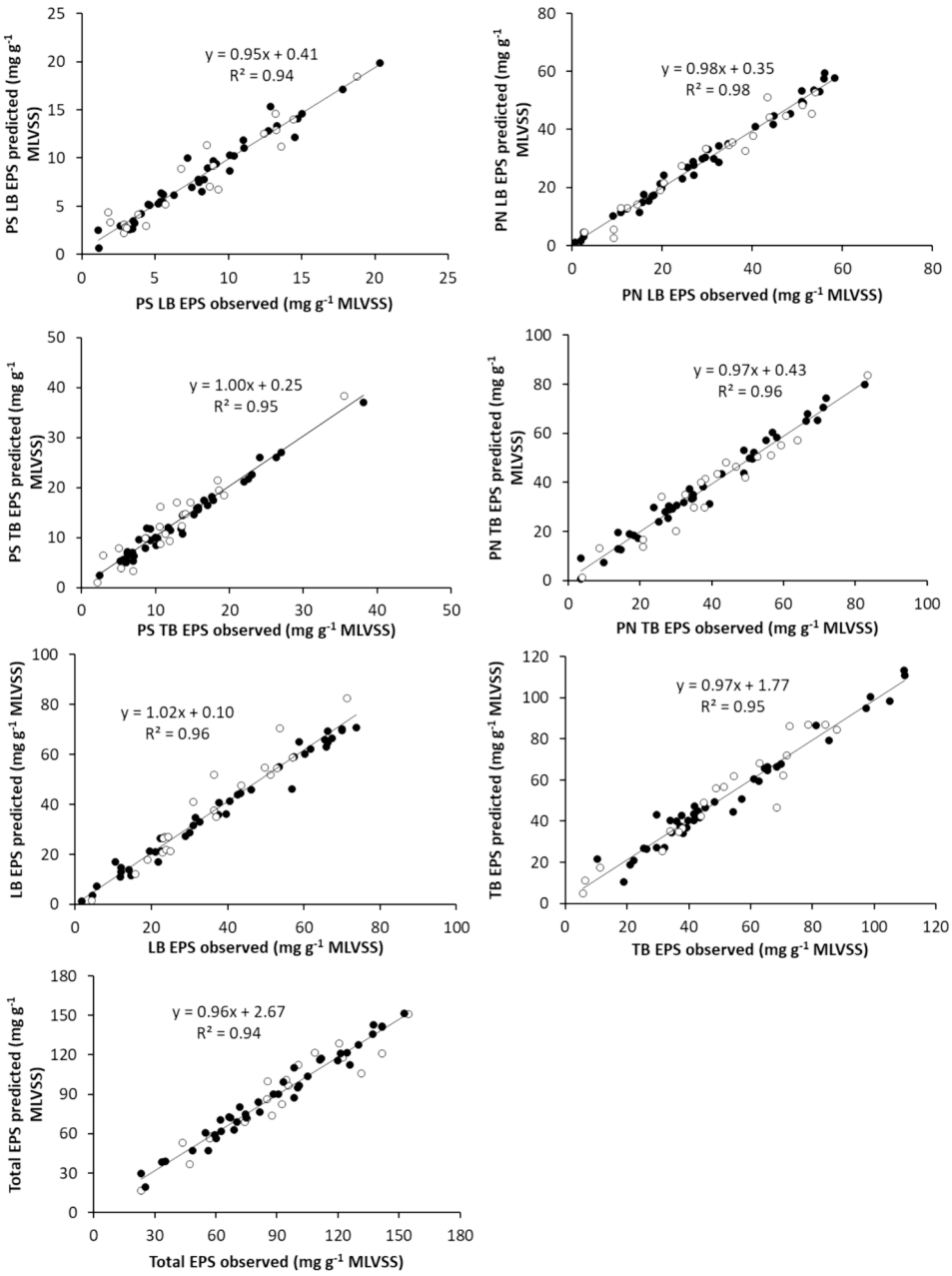

Fig. 3. Regression models (training + validation) for the ensemble of the individually obtained results for each phase. The black dots (●) represent the training set, and white dots (○) represent the validation set.

Data availability

Data will be made available on request.

Acknowledgements

The authors thank the Portuguese Foundation for Science and Technology (FCT) under the scope of the strategic funding of UIDB/04469/2020 unit, and by LABBELS – Associate Laboratory in Biotechnology, Bioengineering and Microelectromechanical Systems, LA/P/0029/2020. The authors also thank the FCT for the financial support to the Research Centre for Natural Resources, Environment and Society — CERNAS (UIDB/00681/2020; DOI: 10.54499/UIDP/00681/2020). Antonio Melo acknowledges Instituto Federal de Educação, Ciência e Tecnologia de Pernambuco (IFPE) funding through the grant number 240-20170220. Cristina Quintelas and Daniela P. Mesquita acknowledge FCT funding under DL57/2016 Transitory Norm Programme and under CEEC INST 2ed (CEECINST/00018/2021/CP2806/CT0004; DOI: 10.54499/CEECINST/00018/2021/CP2806/CT0004), respectively.

Appendix A. Supplementary material

Supplementary material to this article can be found online at https://doi.org/10.1016/j.seppur.2024.127831.

References

[1] V. Kumar, S. Kaur, S. Singh, N. Upadhyay, Unexpected formation of N′-phenyl-thiophosphorohydrazidic acid O, S-dimethyl ester from acephate: chemical, biotechnical and computational study, 3 Biotech 6 (2016) 1–11, https://doi.org/10.1007/s13205-015-0313-6.

[2] A. Sharma, V. Kumar, B. Shahzad, M. Tanveer, G.P.S. Sidhu, N. Handa, S.K. Kohli, P. Yadav, A.S. Bali, R.D. Parihar, O.I. Dar, K. Singh, S. Jasrotia, P. Bakshi,

M. Ramakrishnan, S. Kumar, R. Bhardwaj, A.K. Thukral, Worldwide pesticide usage and its impacts on ecosystem, SN Appl. Sci. 1 (2019) 1446, https://doi.org/10.1007/s42452-019-1485-1.
[3] R. Loos, G. Locoro, S. Comero, S. Contini, D. Schwesig, F. Werres, P. Balsaa, O. Gans, S. Weiss, L. Blaha, M. Bolchi, B.M. Gawlik, Pan-European survey on the occurrence of selected polar organic persistent pollutants in ground water, Water Res. 44 (2010) 4115–4126, https://doi.org/10.1016/j.watres.2010.05.032.
[4] S.C. Stradtman, J.L. Freeman, Mechanisms of neurotoxicity associated with exposure to the herbicide atrazine, Toxics 9 (2021), https://doi.org/10.3390/toxics9090207.
[5] Y. Luo, W. Guo, H. Hao, L. Duc, F. Ibney, J. Zhang, S. Liang, X.C. Wang, A review on the occurrence of micropollutants in the aquatic environment and their fate and removal during wastewater treatment, Sci. Total Environ. 473–474 (2014) 619–641, https://doi.org/10.1016/j.scitotenv.2013.12.065.
[6] L. Goodwin, C. I, C. P, S. A, Treatment options for reclaiming wastewater produced by the pesticide industry, Int. J. Water Wastewater Treatm. 4 (2018), https://doi.org/10.16966/2381-5299.149.
[7] J. Wingender, I. Thomas, R. Neu, H.-C. Flemming, What are bacterial extracellular polymeric substances?, in: Microbial Extracellular Polymeric Substances Springer-Verlag Berlin Heidelberg, 1999, pp. 1–19.
[8] P.H. Santschi, C. Xu, K.A. Schwehr, P. Lin, L. Sun, W.C. Chin, M. Kamalanathan, H. P. Bacosa, A. Quigg, Can the protein/carbohydrate (P/C) ratio of exopolymeric substances (EPS) be used as a proxy for their 'stickiness' and aggregation propensity? Mar. Chem. 218 (2020) 103734 https://doi.org/10.1016/j.marchem.2019.103734.
[9] C. Xu, S. Zhang, C.Y. Chuang, E.J. Miller, K.A. Schwehr, P.H. Santschi, Chemical composition and relative hydrophobicity of microbial exopolymeric substances (EPS) isolated by anion exchange chromatography and their actinide-binding affinities, Mar. Chem. 126 (2011) 27–36, https://doi.org/10.1016/j.marchem.2011.03.004.
[10] T. Yu, L. Wang, F. Ma, J. Yang, S. Bai, J. You, Self-immobilized biomixture with pellets of Aspergillus niger Y3 and Arthrobacter. sp ZXY-2 to remove atrazine in water: A bio-functions integration system, Sci. Total Environ. 689 (2019) 875–882, https://doi.org/10.1016/j.scitotenv.2019.06.313.
[11] M. Gao, R. Liu, B. Li, W. Wei, Y. Zhang, Characteristics of extracellular polymeric substances and soluble microbial products of activated sludge in a pulse aerated reactor, Environ. Technol. (United Kingdom) 41 (2020) 2500–2509, https://doi.org/10.1080/09593330.2019.1573849.
[12] X.Y. Li, S.F. Yang, Influence of loosely bound extracellular polymeric substances (EPS) on the flocculation, sedimentation and dewaterability of activated sludge, Water Res. 41 (2007) 1022–1030, https://doi.org/10.1016/j.watres.2006.06.037.
[13] G.P. Sheng, H.Q. Yu, X.Y. Li, Extracellular polymeric substances (EPS) of microbial aggregates in biological wastewater treatment systems: A review, Biotechnol. Adv. 28 (2010) 882–894, https://doi.org/10.1016/j.biotechadv.2010.08.001.
[14] D.P. Mesquita, A.L. Amaral, E.C. Ferreira, Estimation of effluent quality parameters from an activated sludge system using quantitative image analysis, Chem. Eng. J. 285 (2016) 349–357, https://doi.org/10.1016/j.cej.2015.09.110.
[15] J.G. Costa, A.M.S. Paulo, C.L. Amorim, A.L. Amaral, P.M.L. Castro, E.C. Ferreira, D. P. Mesquita, Quantitative image analysis as a robust tool to assess effluent quality from an aerobic granular sludge system treating industrial wastewater, Chemosphere 291 (2022), https://doi.org/10.1016/j.chemosphere.2021.132773.
[16] APHA, Standard methods for the examination of water and wastewater: 20th ed., American P, 1998.
[17] C. Quintelas, A. Melo, M. Costa, D.P. Mesquita, E.C. Ferreira, A.L. Amaral, Environmentally-friendly technology for rapid identification and quantification of emerging pollutants from wastewater using infrared spectroscopy, Environ. Toxicol. Pharmacol. 80 (2020) 103458, https://doi.org/10.1016/j.etap.2020.103458.
[18] B. Frølund, T. Griebe, P.H. Nielsen, Enzymatic activity in the activated-sludge floc matrix, Appl. Microbiol. Biotechnol. 43 (1995) 755–761, https://doi.org/10.1007/BF00164784.
[19] W. Chen, P. Westerhoff, J.A. Leenheer, K. Booksh, Fluorescence excitation-emission matrix regional integration to quantify spectra for dissolved organic matter, Environ. Sci. Tech. 37 (2003) 5701–5710, https://doi.org/10.1021/es034354c.
[20] A. Melo, J. Costa, C. Quintelas, E.C. Ferreira, D.P. Mesquita, Effects of desloratadine on activated sludge: Behaviour of EPS and sludge properties, J. Environ. Chem. Eng. 10 (2022), https://doi.org/10.1016/j.jece.2022.108415.
[21] A.L. Amaral, Image analysis in biotechnological processes: applications to wastewater treatment, (2003). http://repositorium.sdum.uminho.pt/handle/1822/4506.
[22] J.W. Einax, H.W. Zwanziger, S. Geiß, Chemometrics in Environmental Analysis, VCH Verlagsgesellshaft, Weinheim, 1997.
[23] Z. Derakhshan, A.H. Mahvi, M.T. Ghaneian, S.M. Mazloomi, M. Faramarzian, M. Dehghani, H. Fallahzadeh, S. Yousefinejad, E. Berizi, M.H. Ehrampoush, S. Bahrami, Simultaneous removal of atrazine and organic matter from wastewater using anaerobic moving bed biofilm reactor: A performance analysis, J. Environ. Manage. 209 (2018) 515–524, https://doi.org/10.1016/j.jenvman.2017.12.081.
[24] S. Nasseri, M.A. Baghapour, Z. Derakhshan, M. Faramarzian, Degradation of atrazine by microbial consortium in an anaerobic submerged biological filter, J. Water Health 12 (2014) 492–503, https://doi.org/10.2166/wh.2014.162.
[25] Q. Kong, X. He, Y. Feng, M.S. Miao, Q. Wang, Y. da Du, F. Xu, Pollutant removal and microorganism evolution of activated sludge under ofloxacin selection pressure, Bioresour. Technol. 241 (2017) 849–856, https://doi.org/10.1016/j.biortech.2017.06.019.
[26] P. Zhang, Y.P. Chen, J.S. Guo, Y. Shen, J.X. Yang, F. Fang, C. Li, X. Gao, G.X. Wang, Adsorption behavior of tightly bound extracellular polymeric substances on model organic surfaces under different pH and cations with surface plasmon resonance, Water Res. 57 (2014) 31–39, https://doi.org/10.1016/j.watres.2014.03.018.
[27] G. Zhou, N. Li, E.R. Rene, Q. Liu, M. Dai, Q. Kong, Chemical composition of extracellular polymeric substances and evolution of microbial community in activated sludge exposed to ibuprofen, J. Environ. Manage. 246 (2019) 267–274, https://doi.org/10.1016/j.jenvman.2019.05.044.
[28] X. Pan, J. Liu, D. Zhang, X. Chen, W. Song, F. Wu, Binding of dicamba to soluble and bound extracellular polymeric substances (EPS) from aerobic activated sludge: A fluorescence quenching study, J. Colloid Interface Sci. 345 (2010) 442–447, https://doi.org/10.1016/j.jcis.2010.02.011.
[29] P.H. Santschi, W.C. Chin, A. Quigg, C. Xu, M. Kamalanathan, P. Lin, R.F. Shiu, Marine gel interactions with hydrophilic and hydrophobic pollutants, Gels 7 (2021) 1–14, https://doi.org/10.3390/gels7030083.
[30] H. Zhang, S. Song, Y. Jia, D. Wu, H. Lu, Stress-responses of activated sludge and anaerobic sulfate-reducing bacteria sludge under long-term ciprofloxacin exposure, Water Res. 164 (2019), https://doi.org/10.1016/j.watres.2019.114964.
[31] R.F. Shiu, M.H. Chiu, C.I. Vazquez, Y.Y. Tsai, A. Le, A. Kagiri, C. Xu, M. Kamalanathan, H.P. Bacosa, S.M. Doyle, J.B. Sylvan, P.H. Santschi, A. Quigg, W. C. Chin, Protein to carbohydrate (P/C) ratio changes in microbial extracellular polymeric substances induced by oil and Corexit, Mar. Chem. 223 (2020) 103789, https://doi.org/10.1016/j.marchem.2020.103789.
[32] B. Bin Wang, Q. Chang, D.C. Peng, Y.P. Hou, H.J. Li, L.Y. Pei, A new classification paradigm of extracellular polymeric substances (EPS) in activated sludge: Separation and characterization of exopolymers between floc level and microcolony level, Water Res. 64 (2014) 53–60, https://doi.org/10.1016/j.watres.2014.07.003.
[33] X. Liang, L. Zhang, S.K. Natarajan, D.F. Becker, Proline mechanisms of stress survival, Antioxid. Redox Signal. 19 (2013) 998–1011, https://doi.org/10.1089/ars.2012.5074.
[34] R. Szewczyk, S. Różalska, J. Mironenka, P. Bernat, Atrazine biodegradation by mycoinsecticide Metarhizium robertsii: Insights into its amino acids and lipids profile, J. Environ. Manage. 262 (2020), https://doi.org/10.1016/j.jenvman.2020.110304.
[35] Z. Zhao, X. Zheng, Z. Han, S. Yang, H. Zhang, T. Lin, C. Zhou, Response mechanisms of Chlorella sorokiniana to microplastics and PFOA stress: Photosynthesis, oxidative stress, extracellular polymeric substances and antioxidant system, Chemosphere 323 (2023), https://doi.org/10.1016/j.chemosphere.2023.138256.
[36] A.G. Geyik, B. Kılıç, F. Çeçen, Extracellular polymeric substances (EPS) and surface properties of activated sludges: effect of organic carbon sources, Environ. Sci. Pollut. Res. 23 (2016) 1653–1663, https://doi.org/10.1007/s11356-015-5347-0.
[37] D. Xu, J. Liu, T. Ma, Y. Gao, S. Zhang, J. Li, Rapid granulation of aerobic sludge in a continuous-flow reactor with a two-zone sedimentation tank by the addition of dewatered sludge, J. Water Process Eng. 41 (2021) 101941, https://doi.org/10.1016/j.jwpe.2021.101941.
[38] Y. Tao, S. Hu, S. Han, H. Shi, Y. Yang, H. Li, Y. Jiao, Q. Zhang, M.S. Akindolie, M. Ji, Z. Chen, Y. Zhang, Efficient removal of atrazine by iron-modified biochar loaded Acinetobacter lwoffii DNS32, Sci. Total Environ. 682 (2019) 59–69, https://doi.org/10.1016/j.scitotenv.2019.05.134.
[39] D. Jenkins, M.G. Richard, G.T. Daigger, Manual on the Causes and Control of Activated Sludge Bulking, Foaming, and Other Solids Separation Problems, CRC Press, 2003. https://doi.org/10.1201/9780203503157.
[40] H. Chen, S. Zhou, T. Li, Impact of extracellular polymeric substances on the settlement ability of aerobic granular sludge, Environ. Technol. 31 (2010) 1601–1612, https://doi.org/10.1080/09593330.2010.482146.
[41] Y. Shen, D.M. Huang, Y.P. Chen, P. Yan, X. Gao, New insight into filamentous sludge bulking during wastewater treatment: Surface characteristics and thermodynamics, Sci. Total Environ. 712 (2020) 135795, https://doi.org/10.1016/j.scitotenv.2019.135795.
[42] B. Jin, B.M. Wilén, P. Lant, A comprehensive insight into floc characteristics and their impact on compressibility and settleability of activated sludge, Chem. Eng. J. 95 (2003) 221–234, https://doi.org/10.1016/S1385-8947(03)00108-6.
[43] V. Sodhi, A. Bansal, M.K. Jha, Effect of extracellular polymeric compositions on in-situ sludge minimization performance of upgraded activated sludge treatment for industrial wastewater, J. Environ. Manage. 306 (2022) 114516, https://doi.org/10.1016/j.jenvman.2022.114516.
[44] Y. Shi, Y. Liu, Evolution of extracellular polymeric substances (EPS) in aerobic sludge granulation: Composition, adherence and viscoelastic properties, Chemosphere 262 (2021) 128033, https://doi.org/10.1016/j.chemosphere.2020.128033.
[45] H.X. Shi, J. Wang, S.Y. Liu, J.S. Guo, F. Fang, Y.P. Chen, P. Yan, New insight into filamentous sludge bulking: Potential role of AHL-mediated quorum sensing in deteriorating sludge floc stability and structure, Water Res. 212 (2022) 118096, https://doi.org/10.1016/j.watres.2022.118096.
[46] X. Liu, J. Liu, D. Deng, R. Li, C. Guo, J. Ma, M. Chen, Investigation of extracellular polymeric substances (EPS) in four types of sludge: Factors influencing EPS properties and sludge granulation, J. Water Process Eng. 40 (2021) 101924, https://doi.org/10.1016/j.jwpe.2021.101924.
[47] C. Yin, F. Meng, G.H. Chen, Spectroscopic characterization of extracellular polymeric substances from a mixed culture dominated by ammonia-oxidizing bacteria, Water Res. 68 (2015) 740–749, https://doi.org/10.1016/j.watres.2014.10.046.
[48] Y. Wang, J. Wang, Z. Liu, X. Huang, F. Fang, J. Guo, P. Yan, Effect of EPS and its forms of aerobic granular sludge on sludge aggregation performance during

granulation process based on XDLVO theory, Sci. Total Environ. 795 (2021) 148682, https://doi.org/10.1016/j.scitotenv.2021.148682.
[49] D. Cozzolino, M.J. Kwiatkowski, M. Parker, W.U. Cynkar, R.G. Dambergs, M. Gishen, M.J. Herderich, Prediction of phenolic compounds in red wine fermentations by visible and near infrared spectroscopy, Anal. Chim. Acta (2004) 73–80, https://doi.org/10.1016/j.aca.2003.08.066.
[50] E. Asensi, D. Zambrano, E. Alemany, D. Aguado, Effect of the addition of precipitated ferric chloride on the morphology and settling characteristics of activated sludge flocs, Sep. Purif. Technol. 227 (2019) 115711, https://doi.org/10.1016/j.seppur.2019.115711.
[51] P.D. Sampson, M. Richards, A.A. Szpiro, S. Bergen, L. Sheppard, T.V. Larson, J. D. Kaufman, A regionalized national universal kriging model using Partial Least Squares regression for estimating annual PM2.5 concentrations in epidemiology, Atmos. Environ. 75 (2013) 383–392, https://doi.org/10.1016/j.atmosenv.2013.04.015.
[52] N.D. Lourenço, F. Paixão, H.M. Pinheiro, A. Sousa, Use of spectra in the visible and near-mid-ultraviolet range with principal component analysis and partial least squares processing for monitoring of suspended solids in municipal wastewater treatment plants, Appl. Spectrosc. 64 (2010) 1061–1067, https://doi.org/10.1366/000370210792434332.